Circulation changes and nutrient concentrations in the late Quaternary Aegean Sea: A nonsteady state concept for sapropel formation

J. S. L. Casford,[1,2] E. J. Rohling,[1] R. Abu-Zied,[1] S. Cooke,[1] C. Fontanier,[3] M. Leng,[4] and V. Lykousis[5]

Received 20 October 2000; revised 17 February 2002; accepted 17 February 2002; published 1 June 2002.

[1] The modern Aegean Sea is an important source of deep water for the eastern Mediterranean. Its contribution to deep water ventilation is known to fluctuate in response to climatic variation on a decadal timescale. This study uses marine micropalaeontological and stable isotope data to investigate longer-term variability during the late glacial and Holocene, in particular that associated with the deposition of the early Holocene dysoxic/anoxic sapropel S1. Concentrating on the onset of sapropel-forming conditions, we identify the start of "seasonal" stratification and highlight a lag in $\delta^{18}O$ response of the planktonic foraminifer *N. pachyderma* to termination T1b as identified in the $\delta^{18}O$ record of *G. ruber*. By use of a simple model we determine that this offset cannot be a function of bioturbation effects. The lag is of the order of 1 kyr and suggests that isolation of intermediate/deep water preceded the start of sapropel formation by up to 1.5 kyr. Using this discovery, we propose an explanation for the major unresolved problem in sapropel studies, namely, the source of nutrient supply required for export productivity to reach levels needed for sustained sapropel deposition. We suggest that nutrients had been accumulating in a stagnant basin for 1–1.5 kyr and that these accumulated resources were utilized during the deposition of S1. In addition, we provide a first quantitative estimate of the diffusive ($1/e$) mixing timescale for the eastern Mediterranean in its "stratified" sapropel mode, which is of the order of 450 years. *INDEX TERMS:* 1050 Geochemistry: Marine geochemistry (4835, 4850); 3030 Marine Geology and Geophysics: Micropaleontology; 3339 Meteorology and Atmospheric Dynamics: Ocean/atmosphere interactions (0312, 4504); 4267 Oceanography: General: Paleoceanography; 4870 Oceanography: Biological and Chemical: Stable isotopes; *KEYWORDS:* sapropel, Mediterranean, Holocene, foraminifera, climate variability

1. Introduction

[2] The present-day Aegean Sea (Figure 1) is an important source of deep water for the eastern Mediterranean [*Lacombe et al.*, 1958; *Miller*, 1963; *Roether et al.*, 1996; *Lascaratos et al.*, 1999]. Aegean Intermediate Water (AEIW) is derived from Levantine Intermediate Water (LIW), with its source in the Rhodes Gyre. As this travels north along the Turkish Coast, prevailing offshore winds allow upwelling of the intermediate water to the surface [*Lascaratos*, 1989; *Yüce*, 1995]. In these shallow eastern shelf areas the AEIW consequently forms a single uniform water mass from the surface to the seafloor. As the upwelled AEIW progresses northward, its salinity continues to increase due to evaporation. Winter winds across the Athos Basin (Figure 1) in the far north further enhance the salinity of AEIW, and this together with winter cooling increases its density. This buoyancy loss drives the formation of Aegean Deep Water (AEDW) [*Bruce and Charnock*, 1965; *Burman and Oren*, 1970; *Theocharis*, 1989; *Yüce*, 1995]. Today, AEDW settles in the deeper parts of the Aegean Basin, below 300 m. Traditionally, AEDW formation was considered of minor importance to the deep water ventilation of the open eastern Mediterranean [*Wüst*, 1961]. However, recent studies show that specific (cold) climatic forcing over the Aegean has throughout the 1990s caused AEDW to replace Adriatic Deep Water (ADW) as the main deep water in the open eastern Mediterranean [*Roether et al.*, 1996; *Samuel et al.*, 1999]. The Aegean's rapid response to atmospheric forcing makes it an ideal case study for the analysis of deep water formation and its relationship with climatic change.

[3] Dramatic deep water ventilation changes on longer timescales are also witnessed in the sedimentary record of the Mediterranean by the presence of sapropels. These dark organic-rich layers are found throughout the eastern Mediterranean. Sapropel formation is related to slowing down of deep water ventilation in response to climate related reductions in buoyancy loss [*Rossignol-Strick et al.*, 1982; *Jenkins and Wiliams*, 1983; *Rossignol-Strick*, 1983, 1985, 1987; *Parisi*, 1987; *Cramp and Collins*, 1988; *Cramp et al.*, 1988; *Perissoratis and Piper*, 1992; *Rohling*, 1994]. These reductions are thought to be caused by changes to much wetter climatic conditions at times of increased Northern Hemisphere insolation (precession cycle minima) [*Rossignol-Strick et al.*, 1982; *Rossignol-Strick*, 1983, 1985; *Rohling and Hilgen*, 1991; *Hilgen*, 1991; *Lourens et al.*, 1996]. In addition to suppression of deep water production, sapropel formation has also been associated with increases in export productivity [*Rohling and Gieskes*, 1989; *De Lange et al.*, 1990; *Rohling*, 1994; *Rohling and Hilgen*, 1991; *Thomson et al.*, 1995; *Cramp and O'Sullivan*, 1999].

[4] Modeling of circulation during deposition of the most recent, Holocene, sapropel (S1) has suggested that relatively small increases in surface buoyancy can lead to suppression of deep water circulation in the eastern Mediterranean. An increase of 20–30% in the freshwater budget is thought to be enough to allow interruption of deep water production [*Myers et al.*, 1998; *Rohling and De Rijk*, 1999; *Rohling*, 1999b]. Using the Myers [*Myers et al.*, 1998] circulation model, the biogeochemical implications of

[1]Southampton Oceanography Centre, Southampton, UK.
[2]Now at Department of Geophysical Science, University of Bristol, Bristol, UK.
[3]Department of Geology and Oceanography, Bordeaux University, UMR 58-05,Talence, France.
[4]Natural Environment Research Council Isotope Geoscience Laboratory, Keyworth, UK.
[5]National Centre for Marine Research, Athens, Greece.

0883-8305/02/2000PA000601$12.00

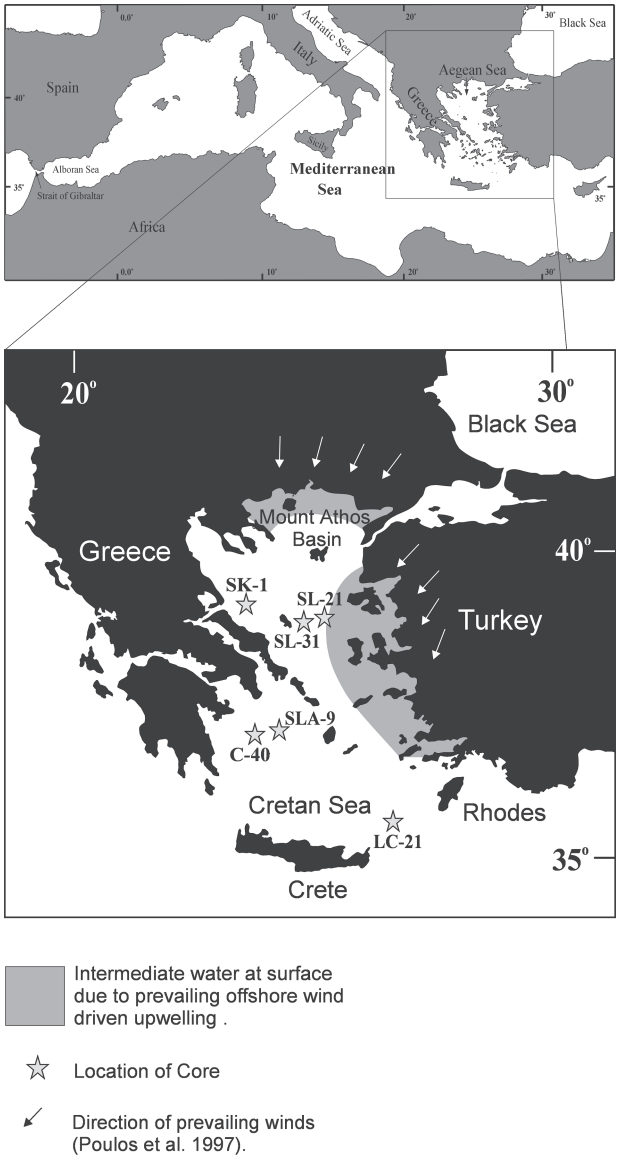

Figure 1. Location map illustrating the core positions for SL-31 (water depth 430 m), SL-21 (317 m), SLA-9 (250 m), and LC-21 (1520 m). The shaded area represents the approximate area of AEIW upwelling to the surface. This water mass extends from the surface to ~200 m depth in the shallow shelf areas off the Turkish coast [*Theocharis*, 1989; *Yüce*, 1995; *Poulos et al.*, 1997].

sapropel formation have been assessed [*Stratford et al.*, 2000]. Preserving the antiestuarine circulation of the eastern Mediterranean and using a threefold increase in river inputs [after *Kallel et al.*, 1997], organic fluxes in coastal regions and marginal basins were found to approach the required levels for sapropel deposition [*Stratford et al.*, 2000].

[5] The model of *Stratford et al.* [2000] highlights a common problem recognized in all current models for sapropel formation, with emphasis on the much studied and well-dated S1: "Where did the nutrients come from to sustain organic matter burial over the ~3 kyr of S1 deposition in the eastern Mediterranean?" It appears that steady state models cannot import sufficient nutrients into the basin, outside of the coastal regions and marginal seas, to sustain this accumulation. The steady state models assume that nutrients lost via C_{org} burial are continuously balanced by fluvial/aeolian influxes. We here present evidence to suggest that the steady state approach is seriously flawed in that a significant period of potential nutrient accumulation in a stagnant basin may have preceded the actual sapropel deposition.

[6] We use abundance variations of planktonic foraminifera together with species-specific oxygen and carbon stable isotope ratios in these forams to derive a picture of the oceanographic processes leading up to, during, and after the most recent sapropel deposition in the Aegean. We observe a conspicuous change in hydrography, starting ~6 kyr prior to S1. We validate our observations with a simple bioturbation model and use the validated records to suggest that long-term (1.5 kyr) storage of nutrients may have occurred in the Aegean Basin. When this reservoir became available for production, the formation of S1 commenced.

2. Methods and Materials

[7] We present results for two gravity cores from the Northern Aegean Basin (SL-21 and SL-31) and an additional gravity core (SLA-9) together with one piston core (LC-21) from the southern Aegean (Figure 1). All four cores are comprised of microfossil-rich hemipelagic ooze, with a clearly defined darker band of sapropelic material.

[8] Each core was sampled in a continuous sequence: SL-21, SL-31, and SLA-9 were sampled at 0.5 cm intervals, and LC-21 was sampled at 1 cm intervals. The samples were freeze-dried and weighed, and selected (weighed) subsamples were disaggregated and wet sieved using demineralized water. The sieved fractions were collected on 600, 150, 125, and 63 μm mesh sizes. The >150 μm fractions were subdivided using a random splitter to provide an aliquot of ~200 individual planktonic foraminifera. These were then determined and sorted on Chapman slides and counted. Results were obtained as numbers g^{-1} and as percentages (Figure 2).

[9] Several AMS radiocarbon dates were obtained for cores LC-21, SLA-9, and SL-31 using only hand-picked clean planktonic foraminiferal tests with no evidence of pyritization or overgrowth. The samples were too small for monospecific dating, but no systematic differences would be expected for such dates relative to our results (see *Jorissen et al.*'s [1993] comparison of planktonic versus benthic dating). The picked material was submitted for analysis at the Natural Environment Research Council (NERC) radiocarbon laboratory at SURRC (LC-21) and at the Leibniz AMS Laboratory at Kiel (Germany) (SLA-9 and SL-31). Radiocarbon convention ages obtained were calibrated using the marine mode of the program Calib 4.2 [*Stuiver and Reimer*, 1993]. A reservoir age correction of 149 ± 30 years for the Aegean was used [*Facorellis et al.*, 1998]. The results are listed in Table 1. All ages in this paper are reported in calibrated kyr B.P. unless otherwise stated.

[10] Detailed stable oxygen and carbon isotope records have been constructed for individual planktonic foraminiferal species in cores LC-21, SLA-9, SL-21, and SL-31, with resolutions on the order of 1 cm (Figure 3). The species chosen were the very shallow, surface-dwelling *Globigerinoides ruber*; the deeper-dwelling *Globorotalia inflata* associated with deep (winter) mixing, and the deep-living species *Neogloboquadrina pachyderma*, which has been associated with the deep chlorophyll maximum at the base of the euphotic layer. This selection follows global and specific Mediterranean habitat descriptions by *Hemleben et al.* [1989], *Pujol and Vergnaud-Grazzini* [1995], *Rohling et al.* [1993a, 1995, 1997], *De Rijk et al.* [1999], and *Hayes et al.* [1999]. The analyses were performed at two separate intercalibrated facilities: the Europa Geo 20−20, with individual acid bath preparation, at the Southampton Oceanography Centre (SOC), and the VG-Optima with a common acid bath preparation at NERC Isotope Geoscience Laboratory (NIGL), Keyworth.

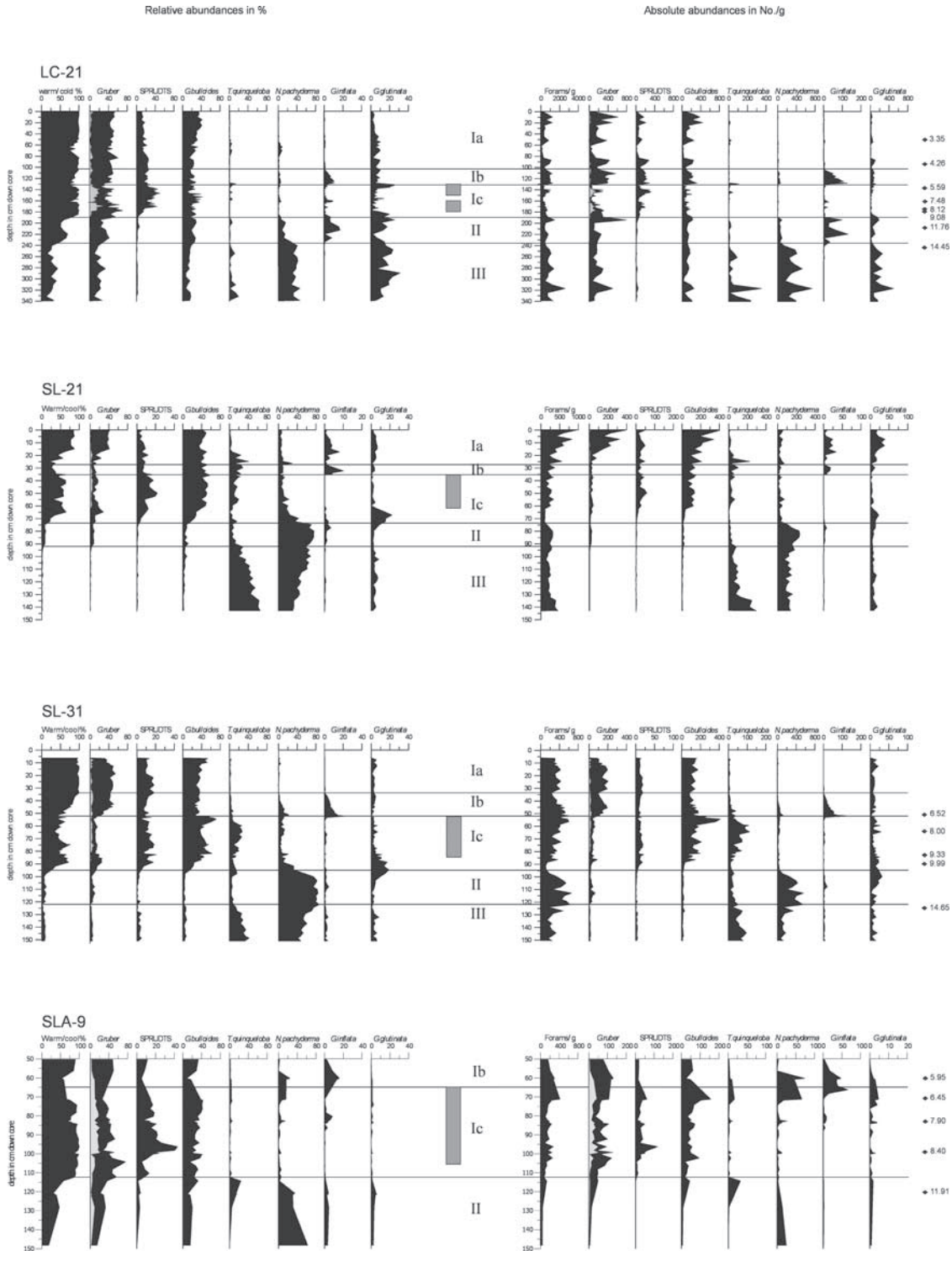

Figure 2. Relative and absolute abundances of planktonic foraminifera in cores SLA-9, SL-21, SL-31, and LC-21. The vertical shaded box indicates the extent of the benthic sapropel, identified from the presence of low-oxygen-tolerant benthic foraminifera and/or total absence of benthic fauna that is equated with truly anoxic bottom waters [*Fontanier*, 2000]. Warm/cold plots are percent warm species/(percent warm + percent cold), following the method of *Rohling et al.* [1997]. The previously defined biozonal boundaries I/II and II/III are also shown [*Jorissen et al.*, 1993]. All dates in Figure 2 are expressed as uncalibrated radiocarbon convention ages, uncorrected for reservoir effect, discussed further in Table 1.

Table 1. Dating Calibration[a]

Sample Code	Median Depth	Conventional Age	± Errors	Calibrated Years B.C.	Calibrated Years B.P.	±1 Sigma
			LC-21			
CAM-41314	50	3370	60	1070	3020	100
CAM-41313	95.5	4290	60	2260	4210	100
CAM-41311	137.5	5590	60	3890	5840	90
CAM-41315	161.5	7480	60	5830	7780	70
CAM-41312	174.25	8120	60	6450	8400	60
AA-30364	179.5	9085	65	7590	9540	320
AA-30365	209	11765	80	11190	13140	370
CAM-41316	242.5	14450	60	14610	16560	240
			SL-31			
KIA9467	51.75	6515	45	4870	6820	70
KIA9468	65.75	7950	60	6330	8280	80
KIA9469	84.25	9330	60	7870	9820	150
KIA9470	91	9990	55	8650	10600	380
KIA9471	126.25	14650	80	14840	16790	250
			SLA-9			
KIA9472	60.5	5950	45	4260	6210	50
KIA9473	71.5	6445	55	4790	6740	70
KIA9474	83.25	7900	45	6240	8190	70
KIA9475	99.5	8400	50	6820	8770	120
KIA9476	120.5	11910	70	11220	13170	350

[a] Dates are show as radiocarbon convention ages (conventional age), calibrated radiocarbon years B.C. (calibrated years B.C.) and as calibrated radiocarbon years B.P. (calibrated years B.P.). Analytical errors are given as years (± errors), and calibration fitting errors for a 1 sigma spread are shown in years (±1 sigma). Dating on LC-21 is after *Mercone et al.* [2000]. Samples with codes starting CAM were prepared as graphite targets at the NERC radiocarbon laboratory and analyzed at the Lawrence Livermore National Laboratory AMS facility. Sample codes AA were prepared at Scottish Universities Reactor Research Centre at East Kilbride and analyzed at the Arizona Radiocarbon Facility. KIA sample codes indicate the Leibniz AMS Laboratory at Kiel. Radiocarbon dating was calibrated using CALIB 4.2 after *Stuiver and Reimer* [1993] and using the marine data set [*Stuiver et al.*, 1998]. A reservoir age correction (ΔR) of 149 ± 30 years was used [*Facorellis et al.*, 1998].

Isotope results are reported as per mil standardized to Vienna Peedee belemnite. Machine error are is of the order of <06‰ (standard deviation).

3. Results

3.1. Planktonic Foraminifera

[11] Five distinct assemblages were identified in this study (Figure 2). The main boundaries equate well with the previously identified biozonal boundary II/III, and biozonal boundary I/II [*Jorissen et al.*, 1993] and this nomennclameture is used. The three remaining assemblages consist of subdivisions of biozone I of *Jorissen et al.* [1993]. Relevant Mediterranean habitat characteristics have been summarized by *Rohling et al.* [1993a, 1993b, 1995], *Pujol and Vergnaud-Grazzini* [1995], *De Rijk et al.* [1999], and *Hayes et al.* [1999]. From old to young we identify the following five assemblages. (1) Assemblage III is an assemblage dominated by *N. pachyderma* and *Turborotalita quinqueloba,* with lower densities of *Globorotalia scitula* and *Globigerinita glutinata*, and a generally low to very low abundance of *G. ruber*. This fauna dominates the cool ''glacial'' intervals. (2) Assemblage II is an intermediate assemblage characterized by presence of *T. quinqueloba*, somewhat enhanced numbers of *N. pachyderma* and *G. glutinata*, especially in the central Aegean cores, and the presence of *G. ruber* and *G. inflata*. (3) Assemblage I is an assemblage dominated by the warm subtropical species *G. ruber* and the SPRUDTS group (including but not requiring *Globigerinella siphonifera, Hastigerina pelagica* (absent in the Aegean), *Globoturborotalita rubescens, Orbulina universa, Globigerinella digitata, Globoturborotalita tenella,* and *Globigerinoides sacculifer* [see *Rohling et al.*, 1993a, 1993b]. In addition it includes abundant *Globigerina bulloides* and somewhat increased *T. quinqueloba* compared with the preceding assemblage II. (4) Assemblage Ic is characterized by elevated absolute and relative abundances of the pink morphotype, *G. ruber* rosa. A peak in *G. inflata* is also present at the base of this assemblage, followed by a marked absence in this species in the remainder of Ic. Core LC-21 shows an interruption in assemblage Ic with a return to a fauna resembling assemblage II, which corresponds to an ''interruption'' of the darker-colored sapropel [*Hayes et al.*, 1999; *De Rijk et al.*, 1999; *Mercone et al.*, 2000]. (5) Assemblages Ib and Ia are diverse assemblages dominated by *G. ruber* and *G. bulloides*, with SPRUDTS, *G. inflata*, and *G. glutinata*. Ib is characterized by elevated numbers of *G. inflata* and appears to be of short duration. Ia shows a fauna similar to that seen in the present-day Mediterranean (core top data of *Thunell* [1978]). Assemblage Ia shows slightly lower abundances of ''warm'' preferring species than assemblage Ic.

3.2. Stable Isotopes

[12] Combination plots of the monospecific isotopic profiles of $\delta^{18}O_{ruber}$, $\delta^{18}O_{inflata}$, and $\delta^{18}O_{pachyderma}$ (Figure 3) show several distinct, previously unreported features: Oxygen isotopes initially show a high degree of synchronicity, being similar in value and variation. This is followed by a depletion in $\delta^{18}O_{ruber}$ that separates it from of the unaffected signal of *N. pachyderma*. This first separation between $\delta^{18}O_{ruber}$ and $\delta^{18}O_{pachyderma}$ coincides with the biozonal boundary III/II and corresponds in age with glacial termination T1a. After a short interval of little change, $\delta^{18}O_{ruber}$ shows a second rapid depletion to its typical Holocene values, while $\delta^{18}O_{pachyderma}$ remains at pre-Holocene values or even shows an enrichment. This enrichment, while generally small, is well within the sensitivity of our equipment and must be regarded as real. It is most obvious in cores SLA-9 (0.8‰ over five samples), SL-21 (0.5‰ over 10 samples), and SL-31 (0.4‰ over four samples), while the available resolution leaves the signal in LC-21 inconclusive in this respect. The $\delta^{18}O$ signal of *G. inflata* shows an inflection to lighter values at the same time as this second depletion in $\delta^{18}O_{ruber}$, while the absolute $\delta^{18}O_{inflata}$ values remain

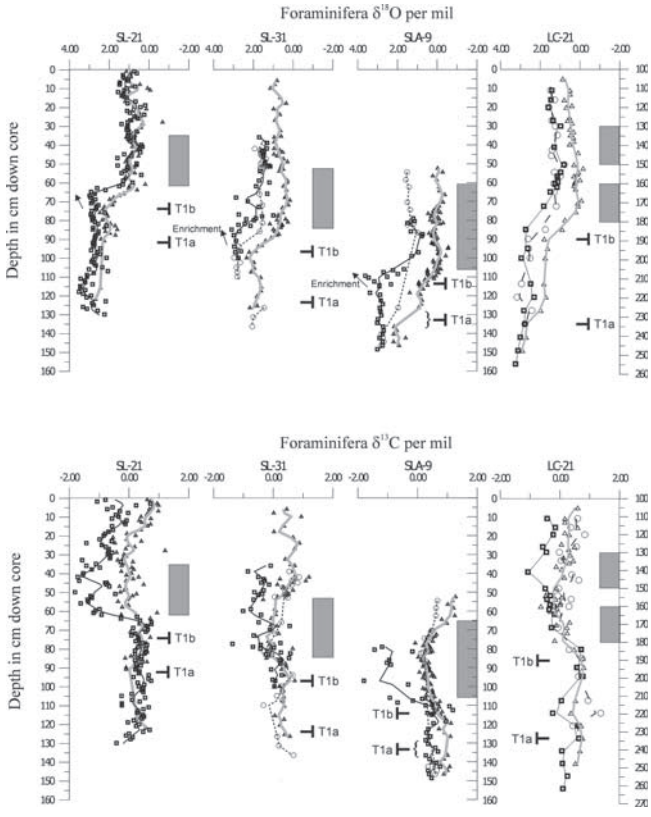

Figure 3. Stable isotope data, showing $\delta^{18}O$ and $\delta^{13}C$ versus depth, for *G. ruber* (thick shaded line with triangles), *N. pachyderma* (thin solid line with squares) and *G. inflata* (dashed line with circles) in cores SLA-9, SL-21, SL-31, and LC-21. The superimposed lines represent a 10 cm running Gaussian smoothing of the data. The shaded boxes represent the extent of the sapropel as defined by the switch from oxygen-requiring benthic foraminifera to the presence of low-oxygen fauna orm in the case of LC-21, the total absence of benthic forams. Glacial terminations T1a and T1b are also shown. Arrows on $\delta^{18}O$ plots of SL-21, SL-31, and SLA-9 indicate enrichment trends in $\delta^{18}O_{pachyderma}$. All values are in per mil versus Vienna Peedee belemnite (‰ VPDB) and calibrated with standards NBS18 and 19.

intermediate between those of $\delta^{18}O_{ruber}$ and $\delta^{18}O_{pachyderma}$. This second sharp depletion in $\delta^{18}O_{ruber}$ equates with termination T1b. Finally, after a period on the order of ~1 kyr, the values of $\delta^{18}O_{pachyderma}$ also start depleting to this species' Holocene values.

[13] Shortly after the start of the depletion in $\delta^{18}O_{pachyderma}$ to Holocene values, we observe a general depletion in $\delta^{13}C$. The $\delta^{13}C$ records show an initial synchronous drop in both $\delta^{13}C_{ruber}$ and $\delta^{13}C_{pachyderma}$, which is followed in SL-21, SL-31, and SLA-9 by a separation of values as $\delta^{13}C_{pachyderma}$ continues to deplete after $\delta^{13}C_{ruber}$ has leveled out. This separation in the $\delta^{13}C$ records coincides with the onset of sapropel deposition.

3.3. Bioturbation Model

[14] The offset in the isotopic responses for $\delta^{18}O_{ruber}$ and $\delta^{18}O_{pachyderma}$ around T1b is conspicuous, and we need to assess whether this is a genuine feature or the result of bioturbation. Owing to the rapid fall in numbers of *N. pachyderma* before the depletion, bioturbation might mix a relatively large proportion of undepleted foraminifera with the comparatively few depleted forams. This could potentially shift the resultant isotopic composition to less depleted values. To test whether such processes could explain the observed trends, we developed a simple model, which assumes a hypothetical step change in the isotopic compositions of both *G. ruber* and *N. pachyderma* at the same point in time. The model then simulates a progressive homogenization (bioturbation) of each successive 0.5 cm of deposited sediment with the previous 5 or 10 cm (separate model runs). Two versions of this simulation were run. An extreme version based on a large step change in numbers of both *G. ruber* and *N. pachyderma* at the same point as the isotopic shift and a run based on the actual numbers observed for these species. The results of the bioturbation model are shown in Figure 4.

[15] All simulations smoothed the imposed step-like $\delta^{18}O$ change into more gradual depletions similar to those seen in the sedimentary record, with differences in the profiles for the two species. However, in all cases the inflection point for the $\delta^{18}O$ values of both species is the same, with both values start to deplete at the same point. This differs markedly from the observed data with a separation in the inflection points of these species by up to >15 cm. Only in our most extreme scenario do we approach the real data, with a lag on the order of 5–10 cm, although even here the infection points are synchronous on closer observation. The models also totally failed to reproduce the enrichment trend in *N. pachyderma* (5–10 data points) that is seen in the actual data during the major depletion in *G. ruber* (this is most clearly seen in cores SL-21, SL-31, and SLA-9).

[16] The bioturbation model leads us to suggest that the actual $\delta^{18}O$ depletion may have been more step-like than is preserved in the sedimentary record. We also deduce that the offset in inflection points seen in our cores reflects a real change in isotopic gradients within the water column during this period.

[17] Interestingly, the signal from *G. inflata* does appear to parallel the *N. pachyderma* signal shape seen in our model. It too sees a marked decline in numbers over the period of isotopic depletion. This signal may therefore provide an indication of the strength of bioturbation below the sapropel, suggesting that homogenization of foraminiferal sized particles due to bioturbation was <5 cm. This would agree with observations in the faunal counts where species *N. pachyderma*, *G. inflata*, and *G. glutinata* fall abruptly to zero in between consecutive samples at 2.5 cm spacing.

4. Discussion

[18] Changes in stable isotope composition have led to considerable speculation on the variability of Mediterranean freshwater budgets [*Huang and Stanley*, 1972; *Cita et al.*, 1977; *Ryan and Cita*, 1977; *Williams et al.*, 1978; *Rossignol-Strick et al.*, 1982; *Thunell and Williams*, 1989; *Kallel et al.*, 1997; *Rohling and De Rijk*, 1999]. Recent work points out that oxygen isotopic ratios from planktonic foraminifera cannot be used to determine absolute salinities in any straightforward way on geological timescales. Rather, they show responses to hydrographic changes that may be several times greater than the corresponding changes in conservative properties, i.e., salinity [*Rohling and De Rijk*, 1999; *Rohling*, 1999a, 1999b]. Such problems associated with temporal gradients are avoided in comparisons of isotopic compositions of different species within an individual sample since foraminifera are then analyzed from an area in a single hydrological regime. Thus differences in the signal between species will reflect real, contemporaneous differences between their preferred habitats.

[19] We propose that our multiproxy records are best interpreted in combination with the foraminiferal abundance records, as a series of successive changing, climatically driven, dynamic regimes. These are illustrated as a series of transitory states together with a schematic summary of the main isotopic and faunal changes recognized in our Aegean records (Figures 5 and 6). Each state represents a single point in time, which may be considered

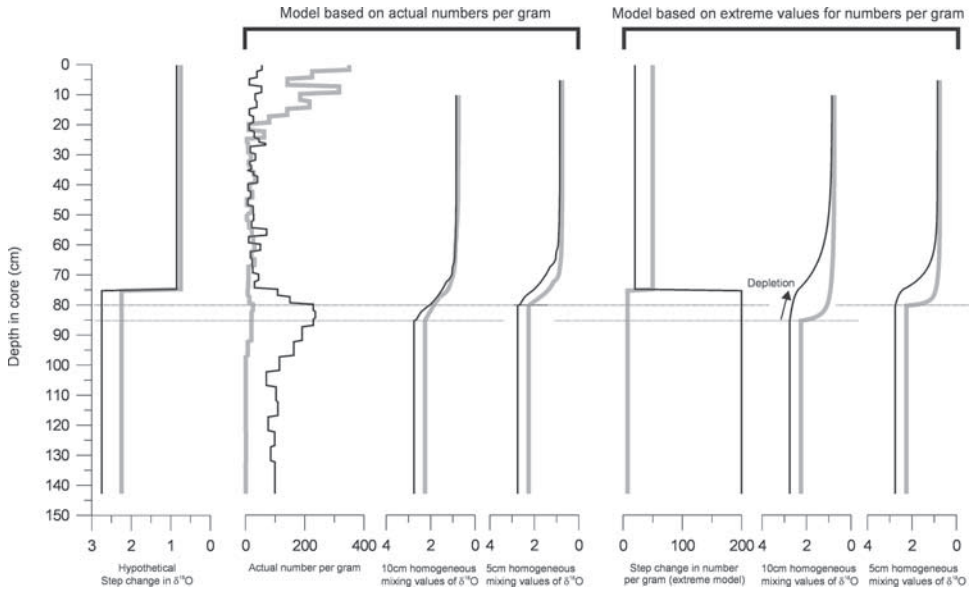

Figure 4. Bioturbation model, which illustrates the smoothing of a hypothetical stepped change in isotopic values (left panel) with a progressive homogenization to simulate bioturbation effects. This includes two runs of the model: one based on the actual numbers per gram of *G. ruber* (thick shaded line) and *N. pachyderma* (thin solid line) found in core SL-21 and another based on a hypothetical extreme step change in numbers per gram, with this change taking place at the same point as the step change in isotopic value. Each version was run with a 5 and a 10 cm homogenization, and these are plotted adjacent to each other for comparison. The horizontal tie lines (dotted lines) highlight the timing of the inflections in the derived $\delta^{18}O$ records.

typical of the particular climatic/circulation regime. These transitory states are described in detail below.

4.1. State A

[20] State A is interpreted as typical of the glacial Aegean Sea. This state is characterized by the absence of warm mixed layer species. We observe coinciding values of $\delta^{18}O_{ruber}$ and $\delta^{18}O_{pachyderma}$ as well as $\delta^{13}C_{ruber}$ and $\delta^{13}C_{pachyderma}$, suggesting that there were no isotopic gradients between these shallow- and subsurface-living species. Thus it is deduced that the water column during state A comprised of a single homogenized water mass, with intermediate water undistinguished from surface water. The presence of *G. inflata* is regarded as indicative of deep seasonal mixing and is hence shown in association with winter mixing [*Hemleben et al.*, 1989; *Rohling et al.*, 1995; *Pujol and Vergnaud-Grazzini*, 1995] (summarized by *Rohling et al.* [1993a] and *Reiss et al.* [2000]). The faunal assemblage comprised of predominantly cool-water species, with only very rare occurrences of the warm dweller *G. ruber. T. quinqueloba* is shown as the principal surface dweller [cf. *Rohling et al.*, 1993a]. *G. scitula* and *N. pachyderma* are shown living at depth. *N. pachyderma* is known to thrive at or just above the base of the euphotic zone and generally prefers stable stratified environments [*Hemleben et al.*, 1989; *Rohling and Gieskes*, 1989; *Rohling et al.*, 1993a, 1995; *Reiss et al.*, 2000]. *G. scitula* in particular is tolerant of low temperatures [*Hemleben et al.*, 1989], and we therefore shown it as present exclusively in winter, although we cannot exclude its possible presence from other seasons on the basis of the data available.

4.2. State B

[21] This state is typical of the regime we believe marks the appearance of distinct seasonal stratification in the post-glacial Aegean. The earliest depletion in $\delta^{18}O_{ruber}$ represents termination 1a. The onset of a separation between the $\delta^{18}O_{ruber}$ and $\delta^{18}O_{pachyderma}$ records suggests that *G. ruber* lived in an isotopically different water mass than *N. pachyderma*. Where available, the $\delta^{18}O_{inflata}$ values clearly follow the $\delta^{18}O_{pachyderma}$ record. Therefore we show these two species in state B as inhabiting the same water mass: *G. inflata* in the deep winter mixed season and *N. pachyderma* below the seasonal thermocline in the previous winter's water. The increased abundance of *G. ruber* over termination 1a itself also indicates the development of seasonal stratification with a warm mixed layer since *G. ruber* has a minimum temperature requirement of ~14°C [*Hemleben et al.*, 1989; *Bijma et al.*, 1990a, 1990b; *Reiss et al.*, 2000]. Hence we infer that termination 1a was associated with significant development/strengthening of the summer thermocline. This is further corroborated by the increase in *N. pachyderma* abundances since this species is known to prevail in stable stratified settings with a well-developed deep chlorophyll maximum [*Hemleben et al.*, 1989; *Rohling and Gieskes*, 1989; *Rohling et al.*, 1993a, 1993b; *Reiss et al.*, 2000]. Plankton tows from the modern NW Mediterranean clearly illustrate *N. pachyderma*'s preference for such hydrographic conditions [*Rohling et al.*, 1995]. The continued presence of the *G. inflata* and its peak in abundance toward the end of biozone II strongly suggests the persistence of seasonal mixing to considerable depth. The shallower-living (~75 m) species *G. glutinata* [*Reiss et al.*, 2000] also occurs in state B. This species is a specialist diatom feeder [*Hemleben et al.*, 1989] and is normally associated with the spring bloom, triggered by the newly available nutrients at the end of winter mixing and increased solar irradiation. Thus we interpret the overall evidence for state B as indicative of seasonal, thermal stratification, alternating with vigorous seasonal overturn of the water column in the colder months.

4.3. State C

[22] State C in particular represents a transitory phase, marking a "snapshot" within the changing conditions from the start of termination 1b to the onset of sapropel production. This regime sees the first occurrence of *O. universa* and other members of the

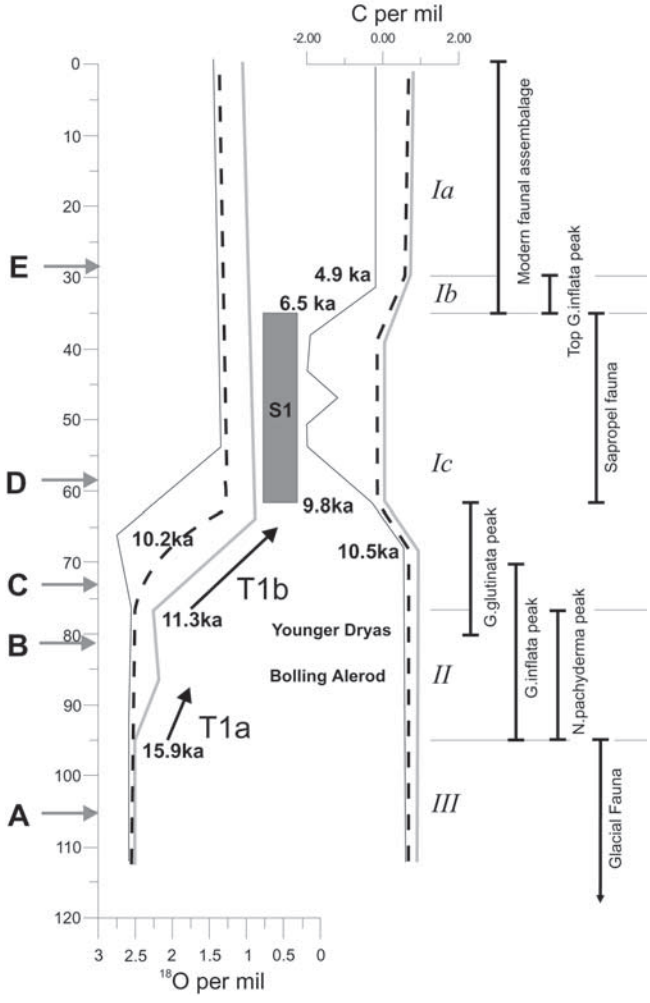

Figure 5. Summary of major changes in isotopic signals $\delta^{18}O$ and $\delta^{13}C$. The thick shaded line indicates $\delta^{18}O_{ruber}$, thin solid line indicates $\delta^{18}O_{pachyderma}$, and the dashed line indicates $\delta^{18}O_{inflata}$. Depth scale is based on core SL-21, and the vertical shaded box indicates the extent of the benthic foraminiferal defined sapropel. Bold letters refer to state summaries in Figure 5. All dates are expressed as calibrated radiocarbon convention ages, corrected for reservoir effect (kyr B.P.) and derived from average ages for the event from cores in this study (Table 2). The hatched area of dysoxic water may be truly anoxic at greater depths (e.g., LC-21, 1500 m). The positions of the Younger Dryas and the Bölling-Alerød are also indicated.

SPRUDTS group. These taxa prefer warm conditions and are shown in Figure 5 above the thermocline. *O. universa* lives in a temperature range of 12°–31°C, and although its photosynthetic symbionts show a dominant habitat in shallower waters, with sufficient light penetration, it can be found down to 250 m, [*Hemleben et al.*, 1989]. We interpret the increase in SPRUDTS and of *G. ruber* as indicative of an increase in depth and extent of the thermocline. The regime in state C is also characterized by the distinct decoupling of the $\delta^{18}O_{ruber}$ and $\delta^{18}O_{pachyderma}$ signals at the biozone I/II boundary, marking an increasing (isotopic) isolation of intermediate/bottom waters from the surface system. There is a synchronous onset of depletions in $\delta^{18}O_{ruber}$ and $\delta^{18}O_{inflata}$, but $\delta^{18}O_{pachyderma}$, on the contrary, responds initially with a small enrichment. As $\delta^{18}O_{inflata}$ inflects with $\delta^{18}O_{ruber}$, we deduce that the winter water ($\delta^{18}O_{inflata}$) responded to the same climatic trend as the summer water ($\delta^{18}O_{ruber}$). This is what would be expected for a substantial perturbation: the effect is seen first and strongest in the shallow summer mixed layer and subsequently passed on to the more voluminous winter mixed layer. Any species living below the summer mixed layer effectively lives in the previous year's winter water, and hence even subsurface summer species should reflect the main isotopic change. However, as $\delta^{18}O_{pachyderma}$ shows a completely independent and opposite response, we infer that *N. pachyderma* lived in a water mass "isolated" from the surface water system. For this reason, we indicate *N. pachyderma* in an intermediate water mass (IW) that was strongly differentiated from the surface system, with the mixing indicators restricted to levels above the IW boundary. Such a condition could have resulted from an invasion of intermediate water from a remote source. Despite the presence of a physically stable environment for *N. pachyderma* we see a rapid reduction in this species' abundance, suggesting that its habitat underwent rapid deterioration. This would fit with our proposal of remotely derived intermediate water since an increase in the pathway from its source relative to the previous locally produced AEIW would result in poorer oxygenation for intermediate water masses in the Aegean. State C also shows a marked reduction in numbers of *G. inflata*, implying that seasonal water column homogenization became inhibited. Shortly following state C, *G. inflata* numbers dwindle into insignificance. The only species showing a real increase is *G. glutinata*. *G. glutinata* may require less dramatic vertical mixing and may hence have replaced *G. inflata*. However, as *G. glutinata* has a short reproductive cycle [*Hemleben et al.*, 1989] it's occurrence may also be an opportunistic response to any increase in nutrient availability. We also identify an increase in numbers of the eutrophic species *G. bulloides*. On the basis of its year-round occurrence in the area today [*Pujol and Vergnaud-Grazzini*, 1995] we have represented it with a year-round occurrence. State C therefore represents a progressive warming of climate and a resulting reduction in local intermediate and deep water production. This allows the increasing isolation of the intermediate water, which in turn allows the

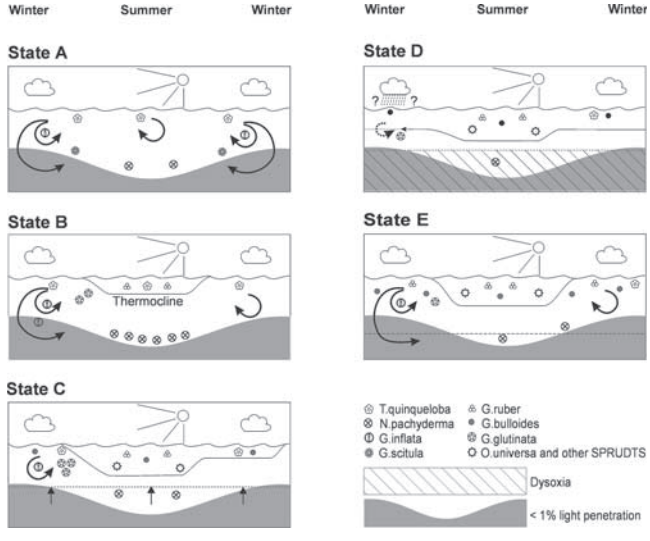

Figure 6. Schematic reconstruction of the history of Aegean circulation. The states illustrated are transitory, and this schematic represents the typical changes in deep water mixing and faunal distribution in the Aegean since the last glaciation. The timing of these transitions and placement of these typical assemblages are summarized in Figure 5.

Table 2. Timing of Events[a]

Event	LC-21, Depth 1520 m	SL-31, Depth 430 m	SK-1	*Geraga et al.* [2000]	SLA-9, Depth 250 m	Mean Age, Calibrated kyr B.P.	Youngest Age, Calibrated kyr B.P.	± (Range/2)
Start of $\delta^{18}O_{ruber}$ depletion T1a	15.7	16.0	–	–	15.9	15.9	15.7	±0.2
III-II	15.8	16.1	15.4	14.8	–	15.5	14.8	±0.6
Start of $\delta^{18}O_{ruber}$ depletion T1b	10.9	11.5	–	–	11.6	11.3	10.9	±0.4
II-Ic	10.9	11.6	11.4	11.1	11.5	11.3	10.9	±0.4
Start $\delta^{13}C$ depletion	10.4	10.3	–	–	10.7	10.5	10.3	±0.2
Start $\delta^{18}O_{pachyderma}$ depletion	10.1	10.2	–	–	10.4	10.2	10.1	±0.2
Age of maximum $\delta^{18}O_{ruber}$ - $\delta^{18}O_{pachyderma}$ difference	10.1	10.2	–	–	10.4	10.2	–	±0.2
Age of level 1/*e* ($\delta^{18}O_{ruber}$ - $\delta^{18}O_{pachyderma}$)	9.85	9.9	–	–	9.55	9.75	–	±0.2
Benthic sapropel	9.5	9.8	–	–	10.1	9.8	9.5	±0.3
End of benthic sapropel	6.1	6.9	–	–	6.4	6.5	6.1	±0.4
Ic-Ib	5.6 (6.1)	6.9	7.1	6.8	6.4	6.6 (6.7)	5.6 (6.1)	±0.8 (±0.5)
Ib-Ia	4.6	5.1	6.1	5.1	–	5.2	4.6	±0.8

[a] This table details the interpolated starting ages of important horizons in cores LC-21, SL-31, and SLA-9. All ages are expressed as calibrated kyr B.P. and are derived by linear interpolation between bracketing dated horizons. The mean age of each event is given in the last column, with the range between cores expressed as an error. Additional dates are given after *Zachariasse et al.* [1997] for core SK1 and *Geraga et al.* [2000] for core C-40. The number in parentheses in the LC-21 column gives the interpolated age of the start of *G. glutinata* increase in LC-21. This also corresponds with the start of benthic reventilation as indicated by an initial reoccurrence of *G. orbicularis*. This point corresponds with an increase of *G. ruber* and a decrease in *T. quinqueloba* and *G. inflata*. We suggest (see text) that the *G. glutinata* increase in the more open setting of LC-21 correlates with the *G. inflata* increase in the more continental settings of the northern Aegean cores.

mineralization products resultant from surface productivity to accumulate in more or less isolated deeper waters.

4.4. State D

[23] This represents the deposition of sapropel S1 and is the culmination of the sequence of changes that started with termination 1b. Roughly 1 kyr after the start of the T1b depletion in $\delta^{18}O_{ruber}$, a similar depletion begins to show up in $\delta^{18}O_{pachyderma}$. The long time lag suggests that diffusive mixing was the major mechanism for transfer of the isotopic depletion from the surface (*G. ruber*) to the deeper environments (*N. pachyderma*) since convective mixing would have caused a virtually instantaneous response between the two species (see, for example, the coincidence between the onsets of depletion in $\delta^{18}O_{ruber}$ and $\delta^{18}O_{inflata}$). The anomalous response of $\delta^{18}O_{pachyderma}$ led us to conclude that it was living subsurface in a water mass unaffected by the local seasonal homogenization (see state C). The $\delta^{13}C_{pachyderma}$ in state D becomes strongly depleted relative to $\delta^{13}C_{inflata}$ and $\delta^{13}C_{ruber}$, suggesting that the strongly reduced *N. pachyderma* population that could survive did so subsurface in an ''isolated'' poorly ventilated water mass with accumulation of ^{12}C-rich remineralization products. We therefore contend that the eventual depletion in $\delta^{18}O_{pachyderma}$ resulted from a slow diffusive mixing process. Our inference of a halt in convective mixing is supported by the presence of dysoxic indicators in the benthic foraminiferal fauna within S1 since a lack of convective overturn results in poor ventilation and consequently dysoxia in bottom waters. For some intervals, at depth (LC-21, 1500 m), no benthic species survive at all, suggesting that bottom waters became totally anoxic. In the planktonic foraminifera, assemblage Ic dominates, which consists of predominately warm-water species with a notable absence of fall/winter/spring mixing indicators. Hence we infer that there was a strongly developed, possibly year-round, thermocline/halocline. During this regime we see depletion in $\delta^{13}C$ for all species recorded. This may be the effect of influx of terrestrial dissolved organic carbon (DOC) [*Asku et al.*, 1999] since this period is known to coincide with a widespread increase in humidity. This is also evidenced by high North African lake levels, high abundance of humidity markers in the local palynological records, and the isotopic anomalies in speleothem data [*Rossignol-Strick*, 1995; *Edmunds et al.*, 1999; *Bar-Matthews et al.*, 1999; *Tzedakis*, 1999; *deMenocal et al.*, 2000]. The resultant increase in freshwater input is schematically represented by a rainfall symbol in state D, even though much of the fresh water would have arrived in the form of river runoff rather than direct precipitation [*Jenkins and Wiliams*, 1983; *Shaw and Evans*, 1984; *Thunell and Williams*, 1989; *Rohling and Hilgen*, 1991; *Rohling*, 1994, 1999b]. As mentioned previously, $\delta^{13}C_{pachyderma}$ depletes more than $\delta^{13}C_{ruber}$ and $\delta^{13}C_{inflata}$, which suggests that such any DOC explanation needs to be combined with the concept that *N. pachyderma* survived in an ageing water mass. With the intermediate water isolated and (virtually) stagnating, it would accumulate an excess of ^{12}C from remineralization. In contrast, the shallow $\delta^{13}C_{ruber}$ signal is continually being equilibrated by contact with the atmosphere. Note that the separation in $\delta^{13}C$ signals coincides with the onset of sapropel formation and therefore with the appearance of benthic markers for very poor bottom water oxygenation, suggesting a culmination of subsurface/deep water stagnation.

4.5. State E

[24] Here we recognize the establishment of a modern circulation regime. The $\delta^{18}O_{pachyderma}$ and $\delta^{18}O_{inflata}$ signals have come back together, suggesting that both live in isotopically undifferentiated winter water. The $\delta^{18}O_{ruber}$ is also similar to $\delta^{18}O_{pachyderma}$ and $\delta^{18}O_{inflata}$ in SL-21 but is slightly more depleted in the remaining cores. This suggests that intermediate and surface waters

in this area are once again very similar, which implies direct local communication between these water masses. This may indicate that (1) intermediate waters are upwelling to the surface and/or (2) surface waters directly contribute to intermediate water formation. Slight $\delta^{13}C$ differentiation between *N. pachyderma* and *G. ruber/G. inflata* suggests that *N. pachyderma* continued to live subsurface at levels more affected by remineralization than the surface/mixed layer environments preferred by *G. ruber* and *G. inflata*. The return of deep mixing indicator *G. inflata* and the presence of the spring bloom indicator *G. glutinata* suggests that seasonal mixing is again well developed. In addition, we see a dominance of *G. bulloides,* giving an overall faunal aspect that is very similar to that seen in modern records [*Thunell*, 1978; *Pujol and Vergnaud-Grazzini*, 1995].

4.6. Deductions on Mechanism and Timing of Circulation Change

[25] Having identified a general trend of reduced potential for deep overturn in the circulatory system during the 6 kyr leading up to sapropel production, we now consider the mechanism and timing of these changes. The trend starts from a glacial environment characterized by a single well-mixed water mass with strong accordance between isotopic signals in all species analyzed. This suggests little density contrast in the water column, while the presence of deep mixing species like *G. inflata* points to regular homogenization/overturn. We have interpreted this as indicative of year-round mixing. This glacial circulation appears to alter with the start of termination 1a. At that time, a shift in environment is clearly indicated in both the fauna and the isotopic data. Our interpolated dates suggest the onset of this change at ~15.9 ka (Table 2). This change associated with T1a appears to have occurred very rapidly, within a few hundred years.

[26] The subsequent regime is characterized by the start/strengthening of summer stratification. We believe this change in circulation was driven by the combination of climatic warming and rising sea levels at the onset of the Bölling-Allerød. During that interval we see the first substantial occurrence of warm mixed layer species, suggesting a general sea surface warming. Together with the increase in *N. pachyderma*, this leads us to suggest the development/strengthening of a stable summer thermocline in a generally well oxygenated environment. Studies of African lake levels and aeolian dust influxes [*Edmunds et al.*, 1999; *deMenocal et al.*, 2000] suggest that this period also saw the start of a regional humidity increase (African humid phase (AHP)). Any increase in freshwater budget would have increased surface buoyancy, helping to establish (seasonal) stratification. This state persisted until the onset of the Younger Dryas (YD) at ~12.5 ka.

[27] In common with many Mediterranean records, the YD is represented in this study by a plateau in the $\delta^{18}O$ records. The fauna shows increases in the mixing indicator *G. inflata* and a decrease in relative abundance of the warm mixed layer species. This suggests a strengthening of winter convection during this period. The YD has also been identified as an interruption in the AHP [*deMenocal et al.*, 2000], and probably represented a cool arid climatic event [*Rossignol-Strick*, 1993, 1995, 1999]. The YD conditions continue until the start of termination 1b marked at ~11.3 ka in our records.

[28] The start of T1b marks a clear dissociation between $\delta^{18}O_{pachyderma}$ and $\delta^{18}O_{ruber}/\delta^{18}O_{inflata}$, from which we deduce that the (intermediate) water mass in which *N. pachyderma* lived was no longer locally connected to the surface system. In addition, we argue that the major source region of intermediate water at this time was somewhere outside of the Aegean. Adriatic intermediate water would be one possible source of our proposed "foreign" intermediate water in the Aegean. This agrees with suggestions of *Myers et al.* [1998] that, the Adriatic Sea was a major source of intermediate water to the eastern Mediterranean during sapropel formation and that this under certain circumstances could enter the Aegean Sea [*Myers and Rohling*, 2000]. This introduction of foreign intermediate water also has implications for the dating of foraminiferal material, a proportion of which will be living in this older water. Correlation between the LC-21 timescale and the GISP II data suggests we see the start of a 350 year offset in LC-21 dates within the anoxic phase. This offset appears to be largely finished by the time of the deposition of the Santorini ash layer [*Rohling et al.*, 2002]. T1b marked the end of the peak in *G. inflata* abundance and a shift toward the dominance of the shallower-living species *G. glutinata* and of warm mixed layer species. This signals the inhibition of deep mixing and the isolation of intermediate waters, corroborating our interpretation of the separation between $\delta^{18}O_{ruber}$ and $\delta^{18}O_{pachyderma}$. From this point on, remineralization products were able to build up in the subsurface to deep waters.

[29] With the ending of the Younger Dryas, the AHP recommenced and persisted until 5.5 ka [*deMenocal et al.*, 2000]. In the Aegean cores we note a depletion in $\delta^{13}C$ for all species analyzed, starting at ~10.5 ka, which we interpret as a possibly the result of increasing humidity in the Aegean Sea. Coinciding with this depletion in $\delta^{13}C$, *G. glutinata* replaces *G. inflata*. This may be tentatively explained in terms of increased freshwater input, which reduced surface buoyancy loss and hence suppressed mixing.

[30] With the suppression of convective mixing in the Aegean, diffusion-type processes become the main driver for property exchange through the water column. At ~10.2 ka, we identify an inflection in $\delta^{18}O_{pachyderma}$, which seems to mark the start of the conveyance of the termination 1b signal to the isolated intermediate water. This allows us to determine a timescale of diffusive mixing. By assessing the time between the maximum $\delta^{18}O_{ruber}$-$\delta^{18}O_{pachyderma}$ gradient and its 1/*e*-fold reduction we can roughly estimate the diffusive timescale for the basin in its stratified sapropel mode. We calculate this to be ~450 years (Table 2).

[31] By ~9.8 ka, deposition of sapropel S1 has commenced (Table 2). This is ~400 years after the total suppression of mixing inferred from the start of the overall $\delta^{13}C$ depletion and the faunal shift to a virtually complete dominance of mixed layer species. The start of sapropel production also occurs ~1500 years after the isolation of the deep/intermediate waters, inferred from the separation of $\delta^{18}O_{ruber}$ and $\delta^{18}O_{pachyderma}$. The isolation of subsurface waters would have allowed subsurface accumulation of remineralization products over a period of up to 1.5 kyr before these products became available for production in the euphotic zone. We suggest that this long-term accumulation provided a major source of excess nutrients that could sustain enhanced productivity during sapropel deposition.

[32] On the basis of benthic foraminiferal indicators, S1 persisted until 6.5 ka (Table 2). At its termination the return of *G. inflata* indicates the restart of seasonal mixing. The warm/cold plots (Figure 2) suggest this may have been a cooling event. In LC-21 the end of the benthic sapropel is marked in the planktonic record by the occurrence of *G. glutinata* first rather than *G. inflata*. This may be related to the proximity of the northern Aegean cores (SL-21 and SL-31) to the area of deep water production in the Athos Basin [*Yüce*, 1995], While the more remote position of LC-21 from the region of water column overturn, would have resulted in a more gradual increase in seasonal mixing, with a correspondingly different progression in the fauna. The general $\delta^{13}C$ depletion may reflect terrestrial DOC influx due to increased humidity persisted until ~4.9 ka. However, the timing of the $\delta^{13}C$ depletion, some 400 years after suppression of mixing, is of the same order as our *e*-fold diffusive timescale, suggesting that the carbon depletion maybe in part due to the upward advective-diffusive transport of ^{13}C-depleted dissolved inorganic carbon (DIC). This DIC would be supplied from deeper waters, depleted in ^{13}C by remineralization.

Around that time the fauna also settled into its modern abundance distributions (Ib-Ia transition, Table 2).

5. Conclusions

[33] There is a clear link between the Aegean hydrographic regime and the global deglaciation phases. Seasonal stratification is weak to nonexistent before the onset of termination 1a, while intermediate water was virtually indistinguishable from shallow waters. After the onset of termination 1a, we identify a distinct seasonal stratification alternating with vigorous overturning seasons. This resulted in a winter mixed layer of similar characteristics to the intermediate water and a summer mixed layer that was distinguished from this by a marked seasonal thermocline. T1b marks the next distinct hydrographic change when intermediate water became dissociated from the summer/winter mixed layers in the study area. This noncommunication between the surface and intermediate system indicates reduced/curtailed ventilation of intermediate and deeper waters. This implies that property exchanges would have become dominated by slow (diffusive) mixing, and we estimate a $1/e$-fold diffusive mixing timescale of $\sim$450 years. This gives the first ever observation-based quantitative estimate of this timescale in the stratified (sapropel mode) Mediterranean.

[34] Furthermore, the dissociation of surface and intermediate systems allowed remineralization products to accumulate in intermediate and deep waters, over a period of up to $\sim$1.5 kyr prior to sapropel deposition. Meanwhile, the isolated intermediate water would have become progressively more dysoxic, a process augmented by the observed increase in (year-round?) stratification. The sapropel therefore appears to represent the culmination of a dynamic nonsteady state process. This has important consequences for the currently accepted steady state approach to circulation and property budget calculations for the eastern Mediterranean in sapropel mode. The sapropel mode ended with the reoccurrence of winter mixing indicative species at $\sim$6.5 ka, while the return to a modern faunal assemblage was completed by $\sim$4.9 ka.

[35] **Acknowledgments.** We thank Frans Jorissen and John Thomson for their constructive comments and discussion, Hilary Sloane for her help with isotopic analysis of cores SL-21 and SL-31 at the NERC Isotope Geoscience Laboratory at Keyworth, UK, and Connie de Vries for her efforts with the stable isotopes of LC-21 at the SOC isotope facility. LC-21 was recovered within EC-MAST2 programme PALAEOFLUX and is held at the BOSCOR repository in Southampton. Aegean cores were collected with the aid of NCMR in Athens, Greece. Data from this paper have been archived with the NOAA-NGDC.

References

Asku, A. E., T. Abrajano, P. J. Mudie, and D. Yaşar, Organic geochemical and palynological evidence for the terrigeneous origin of the organic matter in Aegean Sea sapropel S1, *Mar. Geol.*, *153*, 303–318, 1999.

Bar-Matthews, M., A. Ayalon, A. Kaufman, and G. J. Wasserburg, The eastern Mediterranean paleoclimate as a reflection of regional events: Soreq cave, Israel, *Earth Planet. Sci. Lett.*, *166*, 85–95, 1999.

Bijma, J., W. W. Faber Jr., and C. Hemleben, Temperature and salinity limits for growths and survival of some planktonic foraminifers in laboratory cultures, *J. Foraminiferal Res.*, *20*, 95–116, 1990a.

Bijma, J., J. Erez, and C. Hemleben, Lunar and semi lunar reproductive cycles in some spinose planktonic foramifers, *J. Foraminiferal Res.*, *20*, 117–127, 1990b.

Bruce, J. G., and H. Charnock, Studies of winter sinking of cold water in the Aegean Sea, *Rapp. Comm. Int. Mer. Medit.*, *18*, 773–778, 1965.

Burman, I., and O. H. Oren, Water outflow close to the bottom from the Aegean, *Cah. Oceanogr.*, *22*, 775–780, 1970.

Cita, M. B., C. Vergnaud-Grazzini, C. Roberts, H. Chamley, N. Ciaranfi, and S. d'Onofri, Paleoclimatic record of a long deep sea core from the eastern Mediterranean, *Quat. Res.*, *8*, 205–235, 1977.

Cramp, A., and M. Collins, A late Pleistocene-Holocene sapropel layer in the in N.W. Aegean Sea eastern Mediterranean, *Geo. Mar. Lett.*, *8*, 19–23, 1988.

Cramp, A., and G. O'Sullivan, Neogene sapropels in the Mediterranean: A review, *Mar. Geol.*, *153*, 11–28, 1999.

Cramp, A., M. Collins, and R. West, Late Pleistocene-Holocene sedimentation in the NW Aegean Sea: A palaeoclimatic palaeoceanographic reconstruction, *Palaeogeogr. Palaeoclimatol. Palaeoecol.*, *68*, 61–77, 1988.

De Lange, G. J., J. J. Middelburg, C. H. Van der Weijden, G. Catalano, G. W. Luther III, D. J. Hydes, J. R. W. Woittiez, and G. P. Klinkhammer, Composition of anoxic hypersaline brines in the Tyro and Bannock Basin, eastern Mediterranean, *Mar. Chem.*, *31*, 63–88, 1990.

deMenocal, P., J. Ortiz, T. Guilderson, J. Adkins, M. Sarnthein, L. Baker, and M. Yarusinsky, Abrupt onset and termination of the African humid period: Rapid climate responses to gradual insolation forcing, *Quat. Sci. Rev.*, *19*, 347–361, 2000.

De Rijk, S., E. J. Rohling, and A. Hayes, Onset of climatic deterioration in the eastern Mediterranean around 7 ky BP; micropalaeontological data from Mediterranean sapropel interruptions, *Mar. Geol.*, *153*, 337–343, 1999.

Edmunds, W. M., E. Fellman, and I. B. Goni, Lakes, groundwater and palaeohydrology in the Sahel of NE Nigeria: Evidence from hydrogeochemistry, *J. Geol. Soc. London*, *156*, 345–355, 1999.

Facorellis, Y., Y. Maniatis, and B. Kromer, Apparent ^{14}C ages of marine mollusk shells from a Greek island: Calculation of the marine reservoir effect in the Aegean Sea, *Radiocarbon*, *40*, 963–973, 1998.

Fontanier, C., Successions ecologiques dea foraminiferes benthiques et planctaniques durant les derniers 13.000 ans en mer Egee, MS. thesis, Bordeaux Univ., Bordeaux, France, 2000.

Geraga, M., S. Tsaila-Monopolis, C. Ioakim, G. Papatheodorou, and G. Ferentinos, Evaluation of palaeoenvironmental changes during the last 18,000 years in the Myrtoon basin, SW Aegean Sea, *Palaeogeogr. Paleoclimatol. Palaeoecol.*, *156*, 1–17, 2000.

Hayes, A., E. J. Rohling, S. De Rijk, D. Kroon, and W. J. Zachariasse, Mediterranean planktonic foraminifera faunas during the last glacial cycle, *Mar. Geol.*, *153*, 239–252, 1999.

Hemleben, C., M. Spindler, and O. R. Anderson, *Modern Planktonic Foraminifera*, 363 pp., Springer-Verlag, New York, 1989.

Hilgen, H. J., Astronomical calibration of Gauss to Matuyama sapropels in the Mediterranean and implication for the geomagnetic polarity time scale, *Earth Planet. Sci. Lett.*, *104*, 226–244, 1991.

Huang, T. C., and D. J. Stanley, Western Alboran Sea; sediment dispersal, ponding and reversal of currents, in *The Mediterranean Sea: A Natural Sedimentation Laboratory*, pp. 521–559, Van Nostrand Reinhold, New York, 1972.

Jenkins, J. A., and D. F. Williams, Nile water as a cause of eastern Mediterranean sapropel formation; evidence for and against, *Mar. Micropaleontol.*, *9*, 521–534, 1983.

Jorissen, F. J., A. Asioli, A. M. Borsetti, L. Capotondi, J. P. de Visser, F. J. Hilgen, E. J. Rohling, K. van der Borg, C. Vergnaud Grazzini, and W. J. Zachariasse, Late Quaternary central Mediterranean biochronology, *Mar. Micropaleontol.*, *21*, 169–189, 1993.

Kallel, N., M. Paterne, J. C. Duplessy, C. Vergnaud-Grazzini, C. Pujol, L. Labeyrie, M. Arnold, M. Fontugne, and C. Pierre, Enhanced rainfall in the Mediterranean region during the last sapropel event, *Oceanol. Acta*, *20*, 697–712, 1997.

Lacombe, H., P. Tchernia, and G. Benoist, Contribution à étude hydrologique de la Mer Egée en période d'été, *Bull. Inf. COEC*, *8*, 454–468, 1958.

Lascaratos, A., Hydrology of the Aegean Sea, *Rep. Meteorol. Oceanogr.*, *40*, 313–334, 1989.

Lascaratos, A., W. Roether, K. Nittis, and B. Klein, Recent changes in deep water formation and spreading in the eastern Mediterranean Sea: A review, *Prog. Oceanogr.*, *44*(1/3), 5–36, 1999.

Lourens, L. J. A., F. J. Antonarakou, F. J. Hilgen, A. A. M. Van Hoof, C. Vergnaud-Grazzini, and W. J. Zachariasse, Evaluation of the Plio-Pleistocene astronomical timescale, *Paleoceanography*, *11*, 391–431, 1996.

Mercone, D., J. Thomson, I. W. Croudace, G. Siani, M. Paterne, and S. Troelstra, Duration of S1, the most recent sapropel in the eastern Mediterranean Sea, as indicated by accelerated mass spectrometry radiocarbon and geochemical evidence, *Paleoceanography*, *15*, 336–347, 2000.

Miller, A. R., Physical oceanography of the Mediterranean Sea: A discourse, *Rapp. Comm. Int. Mer Medit.*, *17*, 857–871, 1963.

Myers, P. G., and E. J. Rohling, Modelling a 200 year interruption of the Holocene sapropel S1, *Quat. Res.*, *53*, 98–104, 2000.

Myers, P. G., K. Hayes, and E. J. Rohling, Modelling the paleao-circulation of the Mediterranean: The Last Glacial Maximum and the Holocene with emphasis on the formation of sapropel S1, *Paleoceanography*, *13*, 586–606, 1998.

Parisi, E., Carbon and oxygen isotope composition of *Globerinoides ruber* in two deep sea cores from the Levantine Basin (eastern Mediterranean), *Mar. Geol.*, *75*, 201–219, 1987.

Perissoratis, C., and J. W. Piper, Age, regional variation, and shallowest occurrence of S1 sapropel in the northern Aegean Sea, *Geo. Mar. Lett.*, *12*, 49–53, 1992.

Poulos, S. E., P. G. Drakopoulos, and M. B. Collins, Seasonal variability in sea surface oceanographic conditions in the Aegean Sea (eastern Mediterranean): An overview, *J. Mar. Syst.*, *13*, 225–244, 1997.

Pujol, A., and C. Vergnaud-Grazzini, Distribution patterns of live planktic foraminifera as related to regional hydrography and productive systems of the Mediterranean Sea, *Mar. Micropaleontol.*, *25*, 187–217, 1995.

Reiss, Z., E. Halicz, and L. Boaz, Late-Holocene foraminifera from the SE Levantine Basin, *Isr. J. Earth Sci.*, *48*, 1–27, 2000.

Roether, W., B. B. Manca, B. Klien, D. Bregant, D. Georgopoulos, V. Beitzel, V. Kovacevic, and A. Luchetta, Recent changes in Eastern Mediterranean Deep Waters, *Science*, *271*, 333–335, 1996.

Rohling, E. J., Review and new aspects concerning the formation of eastern Mediterranean sapropels, *Mar. Geol.*, *122*, 1–28, 1994.

Rohling, E. J., Paleosalinity: Confidence limits and future applications, *Mar. Geol.*, 1999a.

Rohling, E. J., Environmental controls on salinity and $\delta^{18}O$ in the Mediterranean, *Paleoceanography*, *14*, 706–715, 1999b.

Rohling, E. J., and S. De Rijk, Holocene climate optimum and the Last Glacial Maximum in the Mediterranean: The marine oxygen isotope record, *Mar. Geol.*, *153*, 57–75, 1999.

Rohling, E. J., and W. W. C. Gieskes, Late Quaternary changes in Mediterranean intermediate water density and formation rate, *Paleoceanography*, *4*, 531–545, 1989.

Rohling, E. J., and F. J. Hilgen, The eastern Mediterranean climate at times of sapropel formation: A review, *Geol. Mijnbouw*, *70*, 253–264, 1991.

Rohling, E. J., F. J. Jorissen, C. Vergnaud-Grazzini, and W. J. Zachariasse, Northern Levantine and Adriatic Quaternary planktic foraminifera; Reconstruction of paleoenvironmental gradients, *Mar. Micropaleontol.*, *21*, 191–218, 1993a.

Rohling, E. J., H. C. de Stigter, C. Vergnaud-Grazzini, and R. Zaalberg, Temporary repopulation by low oxygen tolerant benthic foraminifera within an upper Pliocene sapropel: Evidence for the role of oxygen depletion in the formation of sapropels, *Mar. Micropaleontol.*, *22*, 207–219, 1993b.

Rohling, E. J., M. Den Dulk, C. Pujol, and C. Vergnaud-Grazzini, Abrupt hydrographic change in the Alboran Sea (western Mediterranean) around 8000 yrs BP, *Deep Sea Res., Part I*, *42*, 1609–1619, 1995.

Rohling, E. J., F. J. Jorissen, and H. C. De Stigter, 200 year interruption of Holocene sapropel formation in the Adriatic Sea, *In J. Micropaleontol.*, *16*, 97–108, 1997.

Rohling, E. J., P. A. Mayewski, R. H. Abu-zied, J. S. L. Casford, and A. Hayes, Holocene atmosphere-ocean interactions: Records from Greenland and the Aegean Sea, *Clim. Dyn.*, *18*, 587–593, 2002.

Rossignol-Strick, M., African monsoons, an immediate response to orbital insolation, *Nature*, *304*, 46–49, 1983.

Rossignol-Strick, M., Mediterranean Quaternary sapropels: An immediate response of the African monsoon to variation of insolation, *Palaeogeogr. Palaeoclimatol. Palaeocol.*, *49*, 237–265, 1985.

Rossignol-Strick, M., Rainy periods and bottom water stagnation initiating brine concentrations, 1, The late Quaternary, *Paleoceanography*, *2*, 330–360, 1987.

Rossignol-Strick, M., Late Quaternary climate in the eastern Mediterranean, *Paleorient*, *19*(1), 135–152, 1993.

Rossignol-Strick, M., Sea-land correlation of pollen records in the eastern Mediterranean for glacial-interglacial transition: Biostratigraphy versus radiometric time-scale, *Quat. Sci. Rev.*, *14*, 893–915, 1995.

Rossignol-Strick, M., The Holocene climatic optimum and pollen records of sapropel 1 in the eastern Mediterranean, 9000–6000 BP, *Quat. Sci. Rev.*, *18*, 515–530, 1999.

Rossignol-Strick, M., W. Nesteroff, P. Olive, and C. Vergnaud-Grazzini, After the deluge: Mediterranean stagnation and sapropel formation, *Nature*, *295*, 105–110, 1982.

Ryan, W. B. F., and M. B. Cita, Ignorance concerning episodes of ocean-wide stagnation, *Mar. Geol.*, *23*, 193–215, 1977.

Samuel, S., K. Haines, S. Josey, and P. G. Myers, Response of the Mediterranean Sea thermohaline circulation to observed changes in the winter wind stress field in the period 1980-1993, *J. Geophys. Res.*, *104*(C4), 7771–7784, 1999.

Shaw, H. F., and G. Evans, The nature, distribution and origin of a sapropelic layer in sediments of the Cilicia Basin, northeastern Mediterranean, *Mar. Geol.*, *61*, 1–12, 1984.

Stratford, K., R. G. Williams, and P. G. Myers, Impact of the circulation on sapropel formation in the eastern Mediterranean, *Global Biogeochem. Cycles*, *14*(2), 683–695, 2000.

Stuiver, M., and P. J. Reimer, Extended ^{14}C data base and revised CALIB 3.0 ^{14}C age calibration program, *Radiocarbon*, *35*, 215–230, 1993.

Stuiver, M., P. J. Reimer, E. Bard, J. W. Beck, G. S. Burr, K. A. Hugen, B. Kromer, F. G. McCormac, J. Plicht, and M. Spurk, *Radiocarbon*, *40*, 1041–1083, 1998.

Theocharis, A., Deep water formation and circulation in the Aegean Sea, *Rep. Meteorol. Oceanogr.*, *40*, 335–359, 1989.

Thomson, J., N. C. Higgs, T. R. S. Wilson, I. W. Croudace, G. J. De Lange, and P. J. M. Van Santvoort, Redistribution and geochemical behaviour of redox-sensitive elements around S1, the most recent eastern Mediterranean sapropel, *Geochim. Cosmochim. Acta*, *59*, 3487–3501, 1995.

Thunell, R. C., Distribution of recent planktonic foraminifera in surface sediments of the Mediterranean Sea, *Mar. Micropaleontol.*, *3*, 147–173, 1978.

Thunell, R. C., and D. F. Williams, Glacial-Holocene salinity changes in the Mediterranean Sea: Hydrographic and depositional effects, *Nature*, *338*, 493–496, 1989.

Thunell, R. C., D. F. Williams, and M. Howell, Atlantic-Mediterranean water exchange during the late Neogene, *Paleoceanography*, *2*, 661–678, 1987.

Tzedakis, P. C., The last climatic cycle at Kopais, central Greece, *J. Geol. Soc. London*, *156*, 425–434, 1999.

Williams, D. F., R. C. Thunell, and J. P. Kennet, Periodic fresh-water flooding and stagnation of the eastern Mediterranean Sea during the late Quaternary, *Science*, *201*, 252–254, 1978.

Yüce, H., North Aegean water masses, *Estuarine Coastal Shelf Sci.*, *41*, 325–343, 1995.

Wüst, G., On the vertical circulation of the Mediterranean Sea, *J. Geophys. Res.*, *66*(10), 3261–3271, 1961.

Zachariasse, W. J., F. J. Jorissen, C. Perissoratis, E. J. Rohling, and V. Tsapralis, Late Quaternary foraminiferal changes and the nature of sapropel S1 in Skopelos Basin, paper presented at 5th Hellenic symposium on Oceanography and Fisheries, Natl. Cent. of Mar. Res., Kavalla, Greece, 15–18 April 1997.

R. Abu-Zied, S. Cooke, and E. J. Rohling, Southampton Oceanography Centre, Waterfront Campus, European Way, Southampton, SO14 3ZH, UK.

J. S. L. Casford, Department of Geophysical Science, University of Bristol, University Road, Bristol BS8 1SS, UK.

C. Fontanier, Department of Geology and Oceanography, Bordeaux University, UMR 58-05, Avenue des Facultes, 33405, Talence cedex, France.

M. Leng, Natural Environment Research Council Isotope Geoscience Laboratory, Keyworth, UK.

V. Lykousis, National Centre for Marine Research, Athens, Greece.